ISSN 2075-1133, Inorganic Materials: Applied Research, 2021, Vol. 12, No. 1, pp. 88–93. © Pleiades Publishing, Ltd., 2021.
Russian Text © The Author(s), 2020, published in Materialovedenie, 2020, No. 5, pp. 15–20.

Emergence of Ferromagnetism in Nanoparticles of $BeTiO_3$ Ceramic with the Perovskite Structure

A. V. Pavlov[a, b], L. I. Kveglis[a, b, *], D. N. Saprykin[b], R. T. Nasibullin[c], A. A. Kalitova[b], D. A. Velikanov[a, d], I. V. Nemtsev[a, d], and N. Kantai[b]

[a] *Siberian Federal University, Krasnoyarsk, 660041 Russia*
[b] *Sarsen Amanzholov East Kazakhstan State University, Ust'-Kamenogorsk, 070000 Republic of Kazakhstan*
[c] *Tomsk State University, Tomsk, 634050 Russia*
[d] *Kirensky Institute of Physics, Siberian Branch, Russian Academy of Sciences, Krasnoyarsk, 660036 Russia*
**e-mail: kveglis@list.ru*

Received April 9, 2019; revised November 11, 2019; accepted January 28, 2020

Abstract—Emergence of ferromagnetism and an increase in the electrical conductance of $BeTiO_3$ beryllium ceramic with the perovskite structure were discovered experimentally. To explain the reason for appearance of the metallic properties, models are proposed, and calculations of the electronic structure of nanoclusters with different short-range order are performed.

Keywords: titanium dioxide nanopowder, rutile structure, beryllium ceramic, magnetic hysteresis, electrical resistance, electronic structure, icosahedral clusters

DOI: 10.1134/S2075113321010330

INTRODUCTION

Transition metal oxides show an excellent range of magnetic, superconducting, and multiferroic phases, which are of great scientific interest and are candidates for innovative platforms in power engineering, safety, electronics, and medical technologies. Atomic-scale superlattices formed of transition metal oxides are especially attractive objects for new physics. In superlattices, new states can emerge at interfaces where dissimilar materials come into contact. Ferroelectric order appears from heterostructures consisting of oxide components with nominally contradictive behavior [1].

The current status of research on the properties of oxide ceramics has the following features: oxide ceramic products enjoy remarkably wide and constantly increasing practical application. Among the well-known oxide materials—BeO, Al_2O_3, MgO, SiO_2, ZrO_2, ThO_2, etc.—the BeO ceramic should be pointed out, since it has a thermal conductivity 3 times higher than that of MgO and 4 to 6 times higher than that of Al_2O_3 ceramic. At present, the BeO ceramic is widely used in the electronics industry for dissipation of heat liberated during operation of radio-engineering elements of functional electronics. The high thermal conductivity, low value of dielectric losses, high electric strength, and high stability of electrophysical properties allow applying the BeO ceramic in high-frequency electronic circuits [2]. The presence of developed interfaces and intergrain interactions and a number of other factors related to the surface properties of BeO can have a significant effect on the physicochemical and performance characteristics of the composite ceramic based on BeO. One of the additives capable of considerably changing the conductive and other properties of the BeO ceramic is titanium dioxide TiO_2.

It is known that introduction of TiO_2 into the BeO ceramic after thermal treatment in a reducing atmosphere is accompanied by a considerable increase in density, mechanical strength, electrical conductance, and capability to absorb electromagnetic radiation in the microwave spectral range [3, 4].

The mechanism of this effect has not been fully established so far. In the process of sintering composite ceramics, beryllium oxide endows TiO_2 with increased density, mechanical strength, and thermal conductivity [4]. At present, the most efficient material showing increased density, mechanical strength, good thermal conductivity, and capability to absorb microwave radiation is the composition BeO + 30 wt % TiO_2 (BT-30), in production of which micron-sized TiO_2 powder is used. Increased values of the mechanical strength, density, electrical conductance, and thermal conductivity, provided that the absorbing characteristics remain the same, are of great interest to the microwave and electronics industry [5–7].

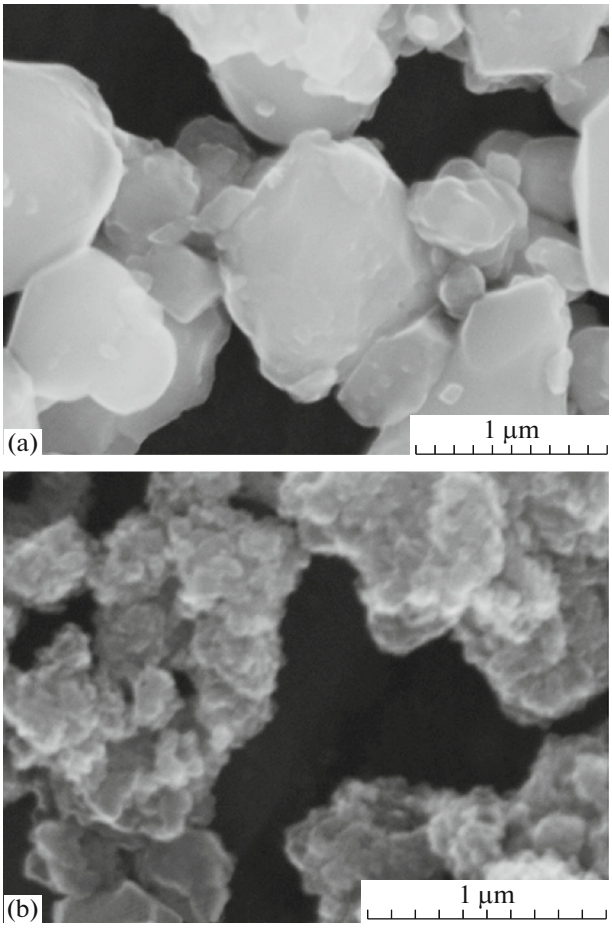

Fig. 1. Images of different TiO_2 powders in scanning electron microscope: (a) micropowder with rutile structure and (b) nanopowder.

In the work, we study the nature of origination and growth of magnetization and conduction in beryllium ceramics as a result of agglomeration when TiO_2 nanopowders are added.

MATERIALS AND METHODS

To track the evolution of structural transformations and other properties of the samples of beryllium oxide ceramics modified with TiO_2 nanopowder, samples with nanopowder additions of 5, 10, 15, 20, 25, and 30 wt % were obtained.

The experimental samples were prepared by slip casting in a heated die mold. The preliminarily annealed starting BeO powder with a specific surface area of 11000 cm^2/g (crystal size from 3 to 10 μm) was mixed with the titanium dioxide nanopowder of the rutile modification (specific surface area of 1.6×10^6 cm^2/g) in an ethyl alcohol medium using a roller mill 3 L in volume and rotary bodies which were balls of beryllium oxide ceramic 15 mm in diameter. The ground powder was chemically purified with the help of a solution of technical-grade hydrochloric acid. After purification, chemical analysis for the content of iron and other impurities was performed. The content of ferromagnetic impurities did not exceed 0.007 wt %.

RESULTS OF INVESTIGATIONS AND THEIR DISCUSSION

Microstructure

Figure 1 shows the micrographs obtained in a scanning electron microscope from the TiO_2 powders: (a) micropowder with the rutile structure and (b) nanopowder.

Figure 2a illustrates the micrograph obtained in a scanning electron microscope from the sintered mixture of the TiO_2 micro- and nanopowders with beryllium dioxide. Figure 2b gives a magnified fragment of this image. Figure 2c displays the image of magnetic contrast from the area illustrated in Fig. 2a. Figure 2d shows the magnetic contrast obtained at a small magnification of the electron microscope in comparison with the contrast from the object holder in the top right corner.

Figure 3 presents the magnetic hysteresis pictures obtained on a vibration magnetometer at room temperature from the beryllium ceramic sintered with the titanium dioxide nanopowder.

X-ray Diffraction Analysis

By means of X-ray diffraction, the structure and phase composition of the beryllium oxide ceramic was investigated in relation to the content of the TiO_2 nanopowder impurity phase. In addition, there was a success in determination of the crystal-geometry schemes of oriented intergrowth between TiO_2 and BeO crystallites leading to formation of an intermediate layer with the perovskite structure.

By interpretation of the X-ray diffraction patterns, orientation relationships which make it possible to reveal an epitaxial connection between TiO_2 and BeO were established. The (210) TiO_2 atomic planes are close to the (101) BeO atomic planes, the (301) TiO_2 atomic planes are close to the (110) BeO atomic planes, the (112) TiO_2 atomic planes are close to the (103) BeO atomic planes, the (321) TiO_2 atomic planes are close to the (200) BeO atomic planes, and the (400) TiO_2 atomic planes are close to the (201) BeO atomic planes (Table 1).

On the basis of interpretation of the X-ray diffraction spectra, it became possible to determine the sizes of octahedral clusters of which the rutile structure is formed (Fig. 4).

The compounds belonging to perovskite-like materials are such that their structure preserves the essential feature of perovskite: skeletons, layers, or rectan-

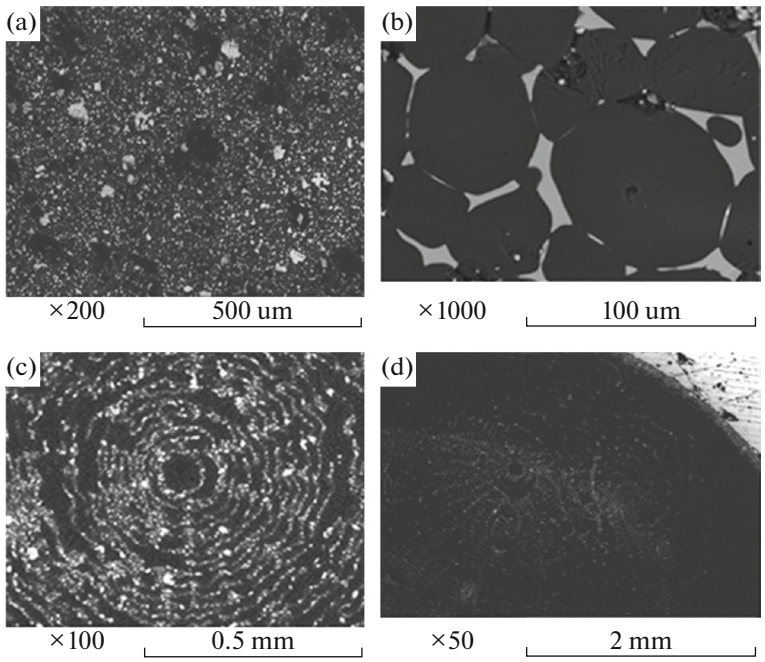

Fig. 2. Scanning electron microscopy images of sintered mixture of TiO_2 micro- and nanopowders with beryllium dioxide: (a) general view of sample; (b) magnified fragment of image (a); (c, d) magnetic contrast from sample shown in Fig. 2a at different magnifications.

gular nets of octahedra, pyramids, or squares are bonded via vertices [8].

Numerous investigations of perovskite-type compounds with the composition ABO_3 demonstrate that such a structure can result even if there is some deviation from conventional notions. For instance, the perovskite-like structure of the beryllium–titanium oxide ceramic based on barium oxide, lithium, and titanium oxide with rhombic distortion, described in [9], includes elements typical of the crystal lattice of tetragonal tungsten bronzes and features the presence of voids—structural vacancies in the barium sublattice.

Currently, the $MTiO_3$–$LnAlO_3$ (M = Ba, Sr, Ca; Ln: La, Sm, Nd) ceramics attract attention among many researchers thanks to the controllable perovskite structure and superior dielectric properties [10, 11].

In our case, in interaction between two crystallites—titanium dioxide and beryllium oxide—mutual penetration and redistribution of oxygen atoms occurs, as a result of which new metal clusters surrounded by oxygen appear.

Comparing the orientation relationships given above, one may claim that epitaxial growth creates an interlayer between TiO_2 and BeO in such a way that the intermediate layer structure corresponds to the perovskite-type structure shown in Fig. 5.

The BeO structure exists in the form of a face-centered cube in which the octahedron is surrounded by the tetrahedra centered with oxygen, so that an oxygen tetrahedron forms.

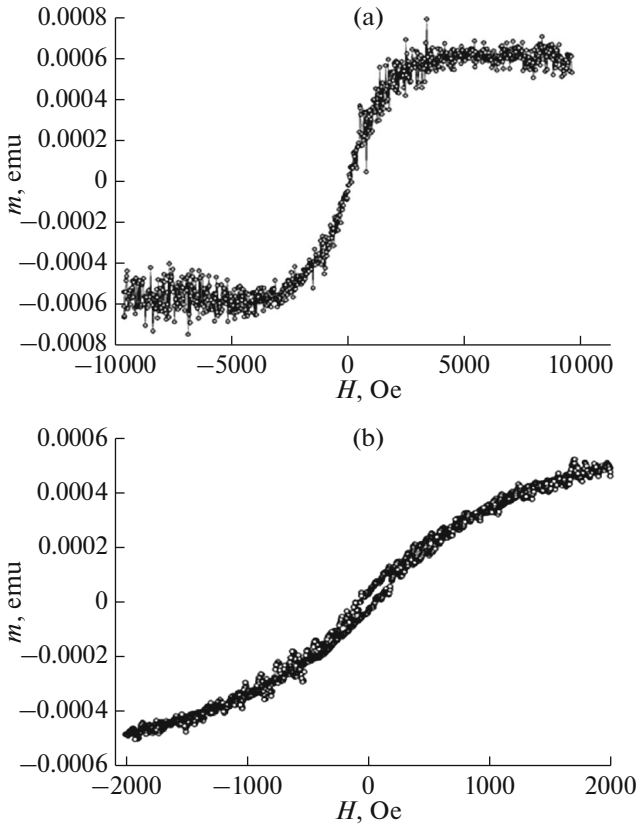

Fig. 3. Magnetic hysteresis loops obtained on vibration magnetometer at room temperature and values of magnetic field H = (a) 10 and (b) 2 kOe.

Table 1. Interpretation of some lines in X-ray diffraction spectrum

No.	2θ	θ	*d*	$d TiO_2$		*d*BeO		Structure
1	43.92	21.96	2.06	2.05	210	2.07	101	$BeTiO_3$
2	69.3	34.9	1.35	1.34	301	1.36	110	$BeTiO_3$
3	77.07	38.54	1.24	1.23	112	1.22	103	$BeTiO_3$
4	82.5	41.25	1.17	1.169	321	1.18	200	$BeTiO_3$
5	84.38	42.19	1.15	1.147	400	1.14	201	$BeTiO_3$

A TiO_2 nanoparticle combining with BeO clusters creates a perovskite crystal structure differing from the classical crystal structure. Figure 6 shows different structural models of the beryllium ceramic—two types of twelve-vertex polyhedra: cuboctahedron (Fig. 6a) and icosahedron (Fig. 6b) of oxygen atoms surrounding a beryllium atom. We determined an icosahedral phase from interpretation of the X-ray diffraction spectra.

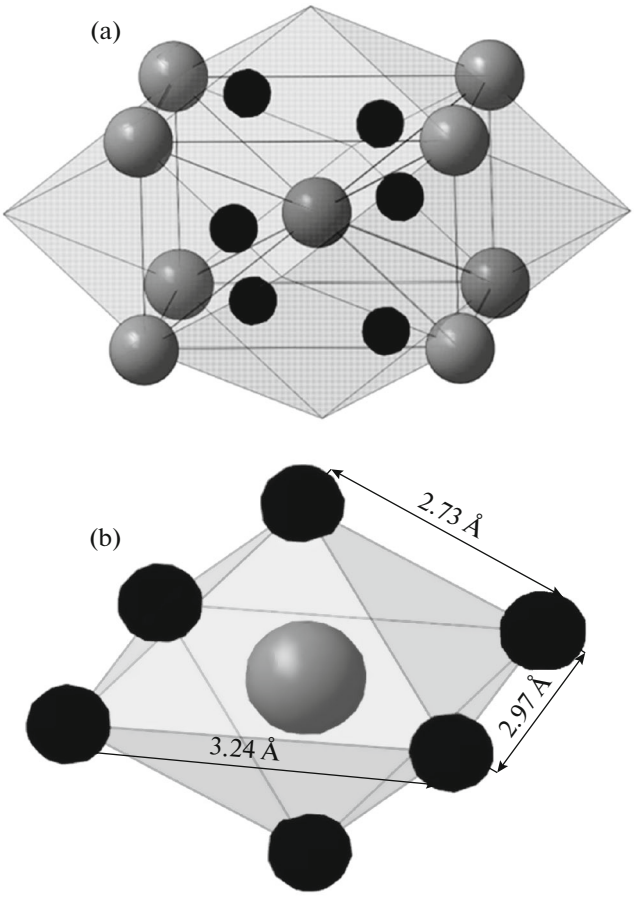

Fig. 4. (a) Cluster rutile structure and (b) octahedral fragment plotted on basis of interpretation of diffraction of X-rays. Titanium atoms are shown in gray and oxygen atoms are shown in black.

The possibility of such structural transformations is described in works by V.S. Kraposhin [11]. When passing from the octahedral to tetrahedral atomic packing, the volume per atom decreases substantially. The octahedron transforms into three tetrahedra, with the volume decreasing by the volume of one tetrahedron. A structure with the minimum free energy results, which is a structure with a conductive phase in the form of a twelve-vertex polyhedron—icosahedron—in which the electron density is much higher owing to a decreased volume per atom. In the icosahedral phase, the electron density on the Fermi level is higher than that in the phase containing a twelve-vertex polyhedron of the classical perovskite.

Using impedance spectroscopy, for the first time, the electrical and dielectric characteristics of this ceramic were studied in the frequency range from 100 Hz to 100 MHz depending on the presence of a micro- and nanosized TiO_2 phase in the composition of the BeO ceramic. It is established that the static resistance of the ceramic with the addition of titanium oxide nanopowder considerably decreases compared to the resistance of the initial ceramic with TiO_2 micropowder [12].

In [13], the nature of ferromagnetism in $BeTiO_3$ perovskite nanoparticles was associated with a high density of structural defects.

In [14], space groups and relationships of the parameters of order and strain (relationships of the parameters of order in ABX_3 perovskite structures)

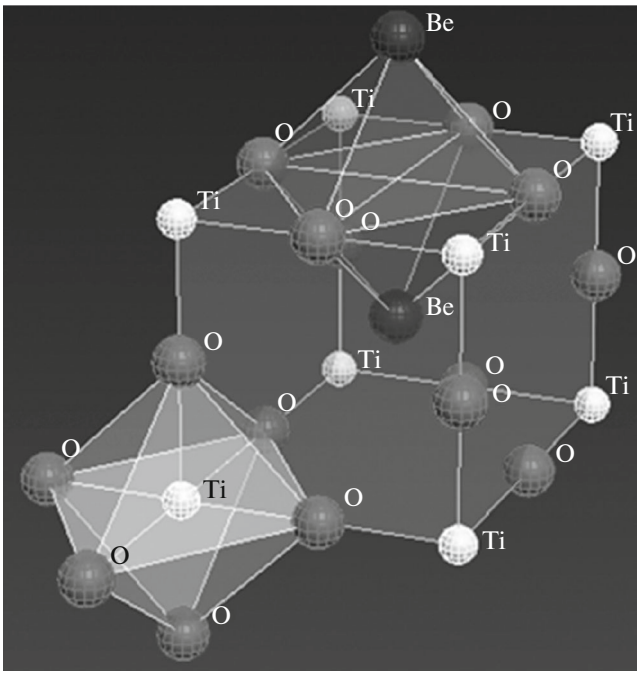

Fig. 5. Crystal structure of dielectric $BeTiO_3$ perovskite phase: at the center, there is a beryllium atom surrounded by twelve oxygen atoms.

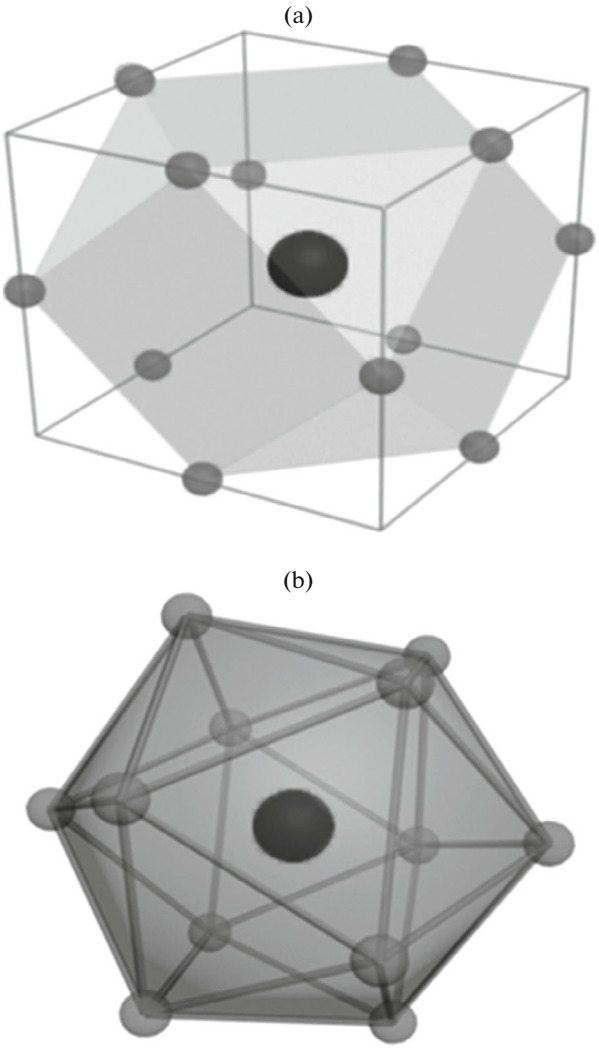

Fig. 6. Two types of twelve-vertex polyhedra in $BeTiO_3$ structure: (a) cuboctahedron and (b) icosahedron.

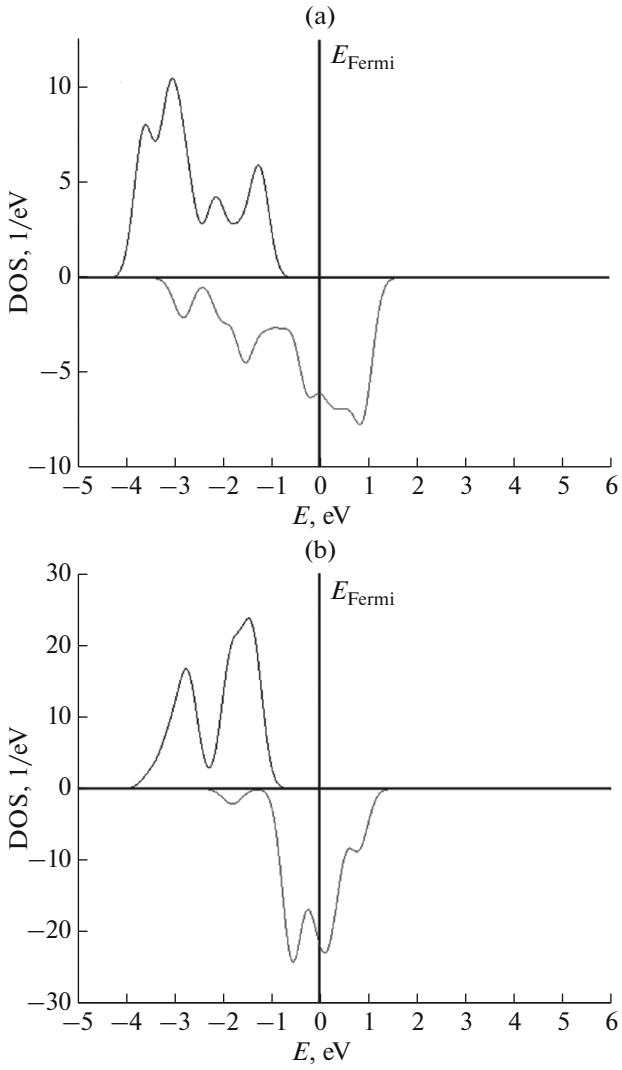

Fig. 7. Density of electronic states for (a) octahedral cluster and (b) icosahedral cluster.

were studied. Parametric coupling and possible phase transitions are described using Landau free-energy expansions.

Electronic Structure Calculation

Investigations of the magnetic properties of clusters formed in the structures based on $BeTiO_3$ were conducted from the perspective of the electron density functional theory (DFT) [15] using a plane wave basis and ultrasoft pseudopotentials [16]. In calculations, the Quantum espresso program package was used [17]. The exchange-correlation functional in a generalized gradient approximation (GGA) was taken in the Perdew–Burke–Ernzerhof (PBE) form [18, 19]. The cutoff energy of the plane-wave basis was assumed to be 60 Ry. The electronic structure was calculated by integrating in the Brillouin zone with the use of the *k*-grid $4 \times 4 \times 4$ constructed according to the Monkhorst–Pack method [20]. The chosen parameters of calculation were determined from investigating the convergence of the total energy and magnetic moment of a cluster with respect to the value of the plane wave basis and partitioning of the Brillouin zone.

For investigating the magnetic properties of the octahedral and icosahedral $BeTiO_3$ phases, a spin-polarized calculation was performed for isolated BeO_6 and BeO_{12} clusters, which are an octahedron and icosahedron, respectively. A Be atom was placed at the center of each cluster, and O atoms were arranged at the vertices. The lengths of the sides for each cluster were 3.24 Å. As a result of calculation, the magnetic moment for the icosahedral (BeO_6) cluster turned out to be $8\mu_B$. In addition, from the analysis of the density of electronic states for each of the considered clusters depicted in Fig. 7, it is seen that appearance of the

magnetic moment is explained by different distributions of the density of electronic states with opposite spins.

Hence, the result of calculation explains the experimentally observed growth in magnetization for the $BeTiO_3$ powders when passing from the octahedral phase to the icosahedral one. Such a result agrees with publication [21], in which strong growth in the electronic states is shown for the icosahedral phase.

CONCLUSIONS

1. The technology of obtaining samples of nanocomposite ceramics with the composition $BeO + TiO_2$ was developed.

2. The evolution of structural phase transformations and the physical properties of beryllium oxide ceramics modified with TiO_2 nanopowder were studied.

3. The features of the physical properties of beryllium ceramics are explained by structural transformations. The icosahedral short-range order creates a high electron density on the Fermi level, which leads to appearance and growth of magnetization of the material.

ACKNOWLEDGMENTS

The images were obtained on Hitachi SU3500 and TM3000 scanning electron microscopes (Kirensky Institute of Physics, Krasnoyarsk Regional Center of Shared Access, Federal Research Center Krasnoyarsk Science Center, Siberian Branch, Russian Academy of Sciences).

FUNDING

The part of the work involving calculations was supported by the Russian Science Foundation (grant no. 18-19-00268).

REFERENCES

1. Chakhalian, J., Freeland, J.W., Millis, A.J., Panagopoulos, C., and Rondinelli, J.M., Colloquium: Emergent properties in plane view: strong correlations at oxide interfaces, *Rev. Mod. Phys.*, 2014, vol. 86, pp. 1189–1202.
2. Kiiko, V.S., Gorbunova, M.A., Makurin, Yu.N., et al., Microstructure and electric conductivity of composite ($BeO + TiO_2$) ceramics, *Refract. Ind. Ceram.*, 2007, vol. 48, no. 6, pp. 429–434.
3. Kiiko, V.S., Dmitriev, I.A., Makurin, Yu.N., et al., Synthesis and application of transparent beryllium ceramics, *Glass Phys. Chem.*, 2004, vol. 30, no. 1, pp. 109–111.
4. Kiiko, V.S., Transparent beryllia ceramics for laser technology and ionizing radiation dosimetry, *Refract. Ind. Ceram.*, 2004, vol. 5, no. 4, pp. 266–272.
5. Kiiko, V.S. and Pavlov, A.V., Composite ($BeO + TiO_2$)-ceramic for electronic engineering and other fields of technology (review), *Refract. Ind. Ceram.*, 2018, vol. 58, no. 5, pp. 1–6.
6. Novikov, A.E., Kiiko, V.S., Kashcheev, I.D., Zuev, M.G., and Zhuravleva, E.Yu., RF Patent 2248336, 2005.
7. Ivanovskii, A.L., Kiiko, V.S., Akishin, G.P., and Makurin, Yu.N., RF Patent 2326091, 2008.
8. Aleksandrov, K.S. and Beznosikov, B.V., Hierarchies of perovskite-like crystals (review), *Phys. Solid State*, 1997, vol. 39, no. 5, pp. 695–715.
9. Nenasheva, E.A., Trubitsyna, O.N., Kartenko, N.F., and Usov, O.A., Ceramic materials for use in microwave electronics, *Phys. Solid State*, 1999, vol. 41, no. 5, pp. 799–801.
10. Yang, X., Wang, X., and Li, L., Effect of MgO on microstructure and microwave dielectric properties of $0.84CaTiO_3$–$0.16Sm_{0.9}Nd_{0.1}AlO_3$ ceramics, *Mater. Res. Bull.*, 2015, vol. 67, pp. 226–229.
11. Kraposhin, V.S., Talis, A.L., and Samoylovitch, M.I., Axial (helical) substructures determined by the root lattice E8 as generating clusters of the condensed phases, *J. Non-Cryst. Solids*, 2007, vol. 353, pp. 3279–3284.
12. Lepeshev, A.A., Pavlov, A.V., and Drokin, N.A., Impedance spectroscopy of ($BeO + TiO_2$)-based ceramics with the addition of TiO_2 nanoparticles, *Zh. Sib. Fed. Univ., Tekh. Tekhnol.*, 2019, no. 3, pp. 366–380.
13. Phan, T.-L., Zhang, P., Yang, D.S., Thanh, T.D., Tuan, D.A., and Yu, S.C., Origin of ferromagnetism in $BaTiO_3$ nanoparticles prepared by mechanical milling, *J. Appl. Phys.*, 2013, vol. 113, pp. 113–117.
14. Carpenter, M.A. and Howard, C.J., Symmetry rules and strain/order-parameter relationships for coupling between octahedral tilting and cooperative Jahn–Teller transitions in *ABX3* perovskites. I. Theory, *Acta Crystallogr., Sect. B: Struct. Sci.*, 2009, vol. 65, pp. 134–146.
15. Giannozzi, P., Baroni, S., Bonini, N., Calandra, M., Car, R., Cavazzoni, C., and Wentzcovitch, R.M., QUANTUM ESPRESSO: a modular and open-source software project for quantum simulations of materials, *J. Phys.: Condens. Matter*, 2009, vol. 21–39, p. 395502.
16. Hohenberg, P. and Kohn, W., Inhomogeneous electron gas, *Phys. Rev. B*, 1964, vol. 136, pp. 864–871.
17. Vanderbilt, D., Soft self-consistent pseudopotentials in a generalized eigenvalue formalism, *Phys. Rev. B*, 1990, vol. 41, pp. 7892–7895.
18. Perdew, J.P., Burke, K., and Ernzerhof, M., Generalized gradient approximation made simple, *Phys. Rev. Lett.*, 1996, vol. 77, pp. 3865–3868.
19. Perdew, J.P., Burke, K., and Ernzerhof, M., Generalized gradient approximation made simple, *Phys. Rev. Lett.*, 1997, vol. 78, pp. 1396–1400.
20. Monkhorst, H.J. and Pack, J.D., Special points for Brillouin-zone integrations, *Phys. Rev. B,* 1976, vol. 13, pp. 5188–5192.
21. Panova, G.H., Chernoplekov, N.A., and Shikov, A.A., Specific heat and electrical resistivity of an icosahedral-structure $Zr_{70}Pd_{30}$ alloy and of its amorphous and crystalline analogs, *Phys. Solid State*, 2005, vol. 47, no. 7, pp. 1205–1210.

Translated by Z. Smirnova